PROCEEDINGS OF SPIE

Simultaneous angular alignment of segmented mirrors using sinusoidal pattern analysis

Heejoo Choi
Isaac Trumper
Matthew   Dubin
Wenchuan   Zhao
Dae Wook Kim

SPIE.

Simultaneous angular alignment of segmented mirrors using sinusoidal pattern analysis

Heejoo Choi,[1] Isaac Trumper, [1] Matthew Dubin,[1] Wenchuan Zhao,[1,2] and Dae Wook Kim[1,3, *]

[1]College of Optical Sciences, Univ. of Arizona, 1630 E. University Blvd., Tucson, AZ 85721, USA;
[2]Chinese Academy of Sciences, The Institute of Optics and Electronics, Chengdu 610209, China;
[3]Steward Observatory, Univ. of Arizona, 933 N. Cherry Ave., Tucson, AZ 85719, USA

ABSTRACT

A segmented mirror is one of the most promising solutions to build an extremely large aperture telescope to reveal the secrets of the universe. In this manuscript, we present a simultaneous angle alignment method for segmented mirrors. By taking the displayed sinusoidal pattern reflecting off the mirrors, the tip-tilt angles are measured with 0.8 µrad resolution for a flat mirror. Due to the efficient calculation using Fourier analysis, the total measurement time for seven flat mirrors is 0.07 s. In addition, a multiplexed sinusoidal pattern is adapted to resolve the intrinsic 2π ambiguity problem in a sinusoidal signal. The presented method can measure any number of segmented mirrors provided that the camera's field of view can cover them all simultaneously.

Keywords: Alignment, Metrology instrumentation, Multi-segmented mirror, Angle measurement, Fourier analysis, Deflectometry.

1. INTRODUCTION

The large aperture telescope is essential for advanced observatory systems [1,2]. A multi-segmented primary mirror is a successful method to achieve large aperture telescopes. This type of primary mirror has an advantage in fabrication and installation compared to a giant single primary mirror [3,4]. However, the segmented type of primary mirror needs a fine alignment for optimum performance. There are various ways to test alignment, each with their own pros and cons.

The image quality can be a criteria of alignment by itself. A point spread function (PSF) is a metric of image quality and can be an indicator for alignment [5], which indirectly senses the orientation of the segments. For every mirror segment, an influence function on the overall PSF is acquired by pre-measurement, which is then used to align the whole set of segments. However, the ambiguity of the segment's influence function increases with the number of segments, which limits the applications for this alignment method. Therefore, a direct test method of detecting misalignment in the mirror segments is desired. The Shack-Hartmann test [6] and curvature sensor [7,8] have been adapted for alignment. The Shack-Hartmann test is sensitive in a tip-tilt measurement, but it is insensitive to local piston motions. The curvature sensor is convenient for a piston alignment test. An interferometric approach can also be a solution for alignment [9]. However, it is limited by a small dynamic range, and a stable environment is required to make a measurement. For a typical angular measurement of a mirror, laser interferometers [10], and photoelectric autocollimators [11] are standard solutions. Their accuracy is state of the art, but they have limited capability when measuring multiple segments and surface shapes. Furthermore, most of the above methods have difficulty when simultaneously measuring many targets.

Deflectometry [12] can be used to align a multi-segmented mirror. To get the alignment result from deflectometry, many calculations such as: phase unwrapping [12], Fourier transforms, filtering and inverse transforms [13], and slope integration [14] are essential. Some advanced versions using instantaneous measurement technology [15] and structured light deflectometry systems [16] also need a complex calculation. However, the complex calculation in deflectometry is superfluous for the tip-tilt angle measurement of a mirror. Moreover, unnecessary calculations accumulate numerical errors. Therefore, a more efficient and intuitive solution is highly desired for less noisy, high dynamic range, and simultaneous applications.

* letter2dwk@hotmail.com
Note: A part of this paper (Section 2, Section 3.1) is mostly based on our recent publication [17].

We present a Simultaneous Multi-segmented mirror Orientation Test System (SMOTS) that uses the deflectometry setup but simplifies the data processing to yield an accurate and efficient alignment. This method provides the orientation information for multiple segments simultaneously and efficiently [17].

2. THEORY

When you see an image through a mirror, the angle of the mirror determines the area where you can see. If you change the tip-tilt angle of the mirror, the image moves. SMOTS uses this simple phenomenon for orientation measurement. If you use a sinusoidal pattern as the image, the image motion produces a phase shift in the sinusoidal pattern, and the tip-tilt angle can be calculated from the phase shift. The parameters necessary for the alignment calculation are the distance between the image pattern and the mirror, and the amount of phase shift due to the misalignment.

The schematic setup for SMOTS is shown in Fig. 1 (left). When starting a measurement, a 2-dimensional sinusoidal pattern is displayed on the screen. A camera then captures an image of this pattern by reflecting off the surfaces under test [Fig. 1 (right)]. Utilizing the hyperfocal condition of the camera allows focusing on both the surface under test and the screen. An initial image is captured to serve as the reference for subsequent measurements. During the tilting of the target mirror, SMOTS measures the shifted image reflecting off the mirror. Once a surface's orientation changes, the linearly shifted sinusoidal pattern is captured by the camera. The amount of deviation from the reference value is converted to the tilt angle by using a sheared pattern analysis. Within the aperture for a single segment (decided by a binary digital mask at the detector plane), the average tilt value is calculated. This calculation is more efficient than conventional deflectometry, which calculates the surface slope at every pixel in the camera. The benefit of averaged calculation within the segment aperture is similar with the Shack-Hartmann wavefront sensor (SHWS) [17]. When measuring a wavefront with the SHWS, the specific size of a single lens in the lenslet array defines the area over which the wavefront is averaged to calculate the slope. Within this area, the SHWS measures the deviated focal point and it converts the deviation to the slope of the wavefront for this territory. Smart sampling and reconstruction of the wavefront in the SHWS simplifies the process and allows real-time measurements. Both methods (SMOTS and SHWS) measure the deviated signal from a reference and then only need simple calculations to determine the target variation. To make an absolute measurement, an "absolute reference" calibration is necessary for SHWS and SMOTS.
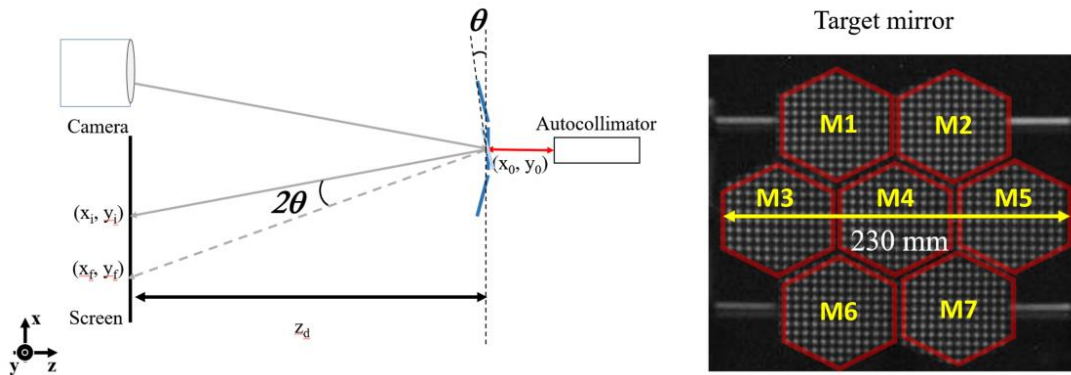

Fig. 1. Schematic diagram of SMOTS setup and picture of segmented target mirror used in experiments. [17]

2.1 Fourier domain data analysis for the sheared fringe

The sheared pattern is obtained by subtracting the reference image from each measured image [Fig 2 (a)-(b)]. The frequency in the sheared patterns contains the same frequency as the reference pattern but with different amplitudes [Fig. 2 (c)]. The amplitude of the sheared patterns directly relates to the extent of shift caused by the change in surface orientation as shown in Fig. 2 (b). The ratio of the amplitude in the frequency domain between the initial (Eq. (1)) and sheared image (Eq. (3)) is used to calculate the amount of phase shift using Eq. (4). In Eqs. (1)–(4), the variable x represents length on the screen in meters, the transform variable f represents frequency (in m^{-1}), and Δ represents the shifted phase when the mirror is moving.

Initial pattern frequency bin: $\qquad FT\big(f(x)\big) = F(f)$ (1)

Shifted pattern frequency bin: $\qquad FT\big(f\,(x + \Delta)\big) = e^{-i2\pi f \Delta} F(f)$ (2)

Sheared pattern frequency bin: $\qquad FT[f(x + \Delta) - f(x)] = FT\big(f(x + \Delta)\big) - FT\big(f(x)\big) = (e^{-i2\pi f \Delta} - 1)\, F(f)$ (3)

The shifted phase Δ : $\qquad \Delta = \dfrac{1}{2\pi f}\cos^{-1}\left[1 - \dfrac{1}{2}\left(\dfrac{\big[FT(f(x+\Delta)) - FT(f(x))\big]^2}{F(f)^2}\right)\right]$ (4)
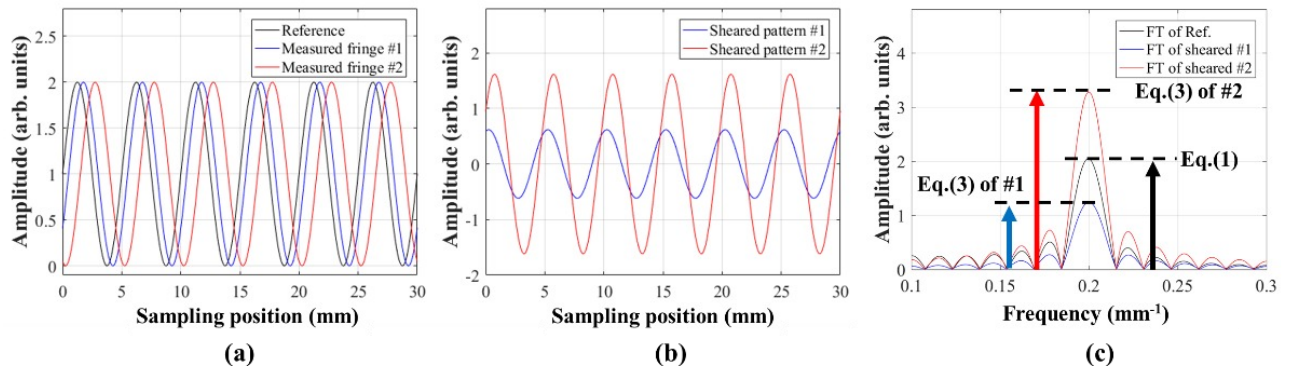

Fig. 2. Data processing steps by using Fourier analysis for sheared pattern. (a) Sinusoidal data with different amount of phase shifts (Blue and Red). (b) Sheared pattern by subtracting the reference data from the shifted data. The amplitude of the sheared pattern is proportional to the phase shift. (c) Fourier transform of the sheared and reference data. The ratio of amplitude in frequency domain gives the amount of phase shift from Eq. (4). [17]

The retrieved phase Δ [Eq (4)] has two limitations. (1) Just like the other sinusoidal pattern-based approaches, there is 2π ambiguity when the shifted phase exceeds a period of one cycle. (2) The other is the directional ambiguity of the phase shift due to the even property of cosine function. For the first issue, a longer period fringe can be utilized to provide a larger dynamic range at the cost of sensitivity for a small angle change. To overcome this tradeoff, we can use multiplexed frequencies to include more information in a single measurement. The multiplexed signal gives a wide dynamic range and retains high resolution. Regarding the second issue, we use the sign of the imaginary component of the Fourier transform to resolve the sign ambiguity of the cosine function. The imaginary parts of two phase shifts equal in magnitude but in different directions are opposite signs at the frequency band of interest.

To measure a physical value, the pixel numbers for one period in the display are used to get a physical length of the phase difference based on the real pixel size as measured under a microscope. The phase Δ in Eq. (4) for the x-axis, gives the position of x_f, defined in Fig. 1 (left) as shown in Eq. (5). The x_i is the initial (i.e., reference) position where the camera looks at the screen.

$$x_f = x_i + \text{Pixel pitch in physical units} \times \text{Number of pixels for one period} \times \text{shifted phase } (\Delta) \qquad (5)$$

The tilt angle θ then can be calculated by

$$\theta = \frac{1}{2}\left(\tan^{-1}\left(\frac{(x_i - x_0)}{z_d}\right) - \tan^{-1}\left(\frac{(x_f - x_0)}{z_d}\right)\right), \qquad (6)$$

where z_d is the distance between the mirror and the screen and x_0 is the mirror position along the x-axis.

Although an aberrated image is acquired by the system, this calculation is still valid since the 2θ deviation of the ray is mostly caused by the tilt angle θ within a small angle regime. Various situations such as spherical mirror measurement, out-of-focus measurement, and off-axis measurement were simulated and verified using Zemax modeling [17].

3. EXPERIMENT AND RESULTS

In order to validate the accuracy and capability of SMOTS, we used seven hexagonal flat mirror segments. The center mirror has two Piezoelectric inertia motors (Thorlabs, PIA25) controlling tip and tilt angles with microradian precision. The other mirrors were attached to kinematic mirror mounts (Thorlabs, KM100). An off-the-shelf monitor (Dell, 1097FP) and camera (Pointgrey, FL3-U3-13Y3M-C) were utilized in the experiment. All measurements were crosschecked with a photoelectric autocollimator (Möller-Wedel, ELCOMAT 3000) as a reference. A binary digital mask was applied to the camera detector image on each mirror segment during the image processing such that only the pattern in each masked area was used to calculate the corresponding mirror orientation change.

3.1 Accuracy and simultaneous capability test

The autocollimator was aligned with a flat mirror [M4 in Fig. 1 (right)], then SMOTS was oriented to see the reflected pattern through the camera. We took an initial picture of the pattern and set this as the reference image because we measure the change in angle from the initial orientation.

We tested SMOTS reliability over a 1.4 mrad range with large angular change steps (~100 µrad). The distance from the mirror to the screen was 2020 ± 5 mm, and the pixel size of the screen was 294 µm. One period of the two-dimensional sinusoidal pattern was set at 30 pixels (8.82 mm). While scanning the mirror angle, the measured angle from both SMOTS and autocollimator were monitored concurrently and compared [Fig. 3]. Ten sets of autocollimator data and fifty SMOTS data sets were acquired to evaluate the performance statistically. As shown in Fig. 3 (right), the difference between the autocollimator and SMOTS is about 0.8 µrad RMS, which is smaller than the noise (error bar) of the data. The dominant noises are random noise at detector and screen such as the white noise of CMOS sensor and the blinking of the monitor.
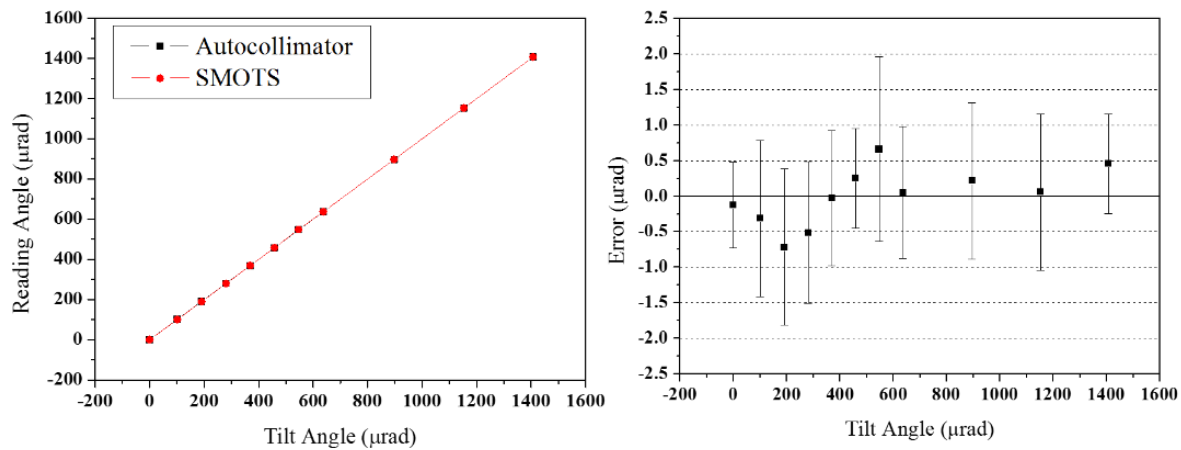

Fig. 3. Measurement result for large dynamic range (left) of SMOTS and autocollimator. The difference between the two measurements (right) shows less than 0.8 µrad RMS errors. (Note: The error bars represents ±1 σ standard deviation for 30 data measurements.) [17]

The simultaneous measurement was demonstrated and evaluated using seven hexagonal mirror segments [17]. To highlight its efficient data processing, a high-speed experiment updating the tip-tilt values at ~15 Hz (with Intel® Xeon® CPU E3 -155M v5, 2.80 GHz) was performed. The most time-consuming process is the image acquisition from the camera.

The simultaneous measurement capability allows us to distinguish the relative orientation data when there is an environmental perturbation. As shown in Fig. 4, an actual change in tilt angle on M4 was applied after 5 s. Meanwhile, a global perturbation was introduced around 12 s and 15 s into the measurement [Two red boxes in Fig. 4]. By monitoring the entire seven segments altogether, the environmental perturbation was clearly recognized as a common motion and compensated for the real M4 orientation change relative to the other segments.
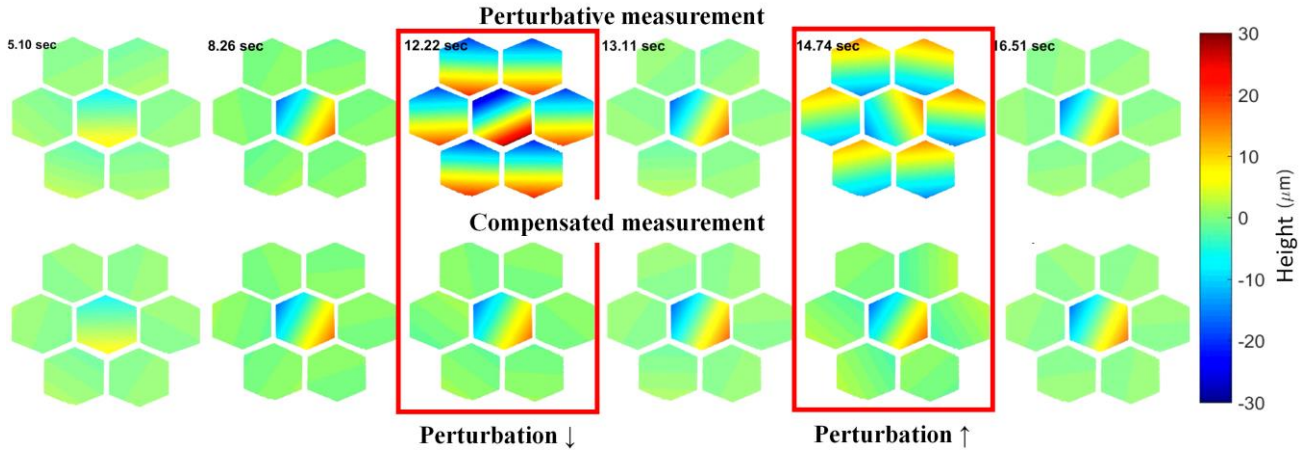
Fig. 4. Time sequence snapshots of simultaneous measurement of the seven hexagonal segments in Fig. 1 (right). A different environmental perturbation was introduced around 12 s and 15 s duration (Red box) [17].

3.2 Multiplexed fringe pattern measurement

The multiplexed signal shown in Fig. 5 (a) is adopted to resolve 2π ambiguity and extend dynamic range. We used the M4 mirror [Fig. 1 (right)] with Piezoelectric inertia motors to give the linear tilting angle variation and the motor's step number was used for the tilt angle calculation as a reference. As shown in Fig. 5 (b), in the frequency domain, the multiplexed fringe pattern clearly shows separated frequency peaks. Also, we picked two specific frequencies f_1 and f_2 in Fig. 5 (b), which have a large LCM (Least Common Multiple) in the frequency domain. The measurement results in Fig. 5 (c) show the 2π ambiguity for each Frequency 1 (e.g., Blue line at the black solid arrow) and Frequency 2 (e.g., Red line at the black dash arrow). However, by combining the information from both frequency data, the thick yellow line overcoming the 2π ambiguity was successfully recovered.
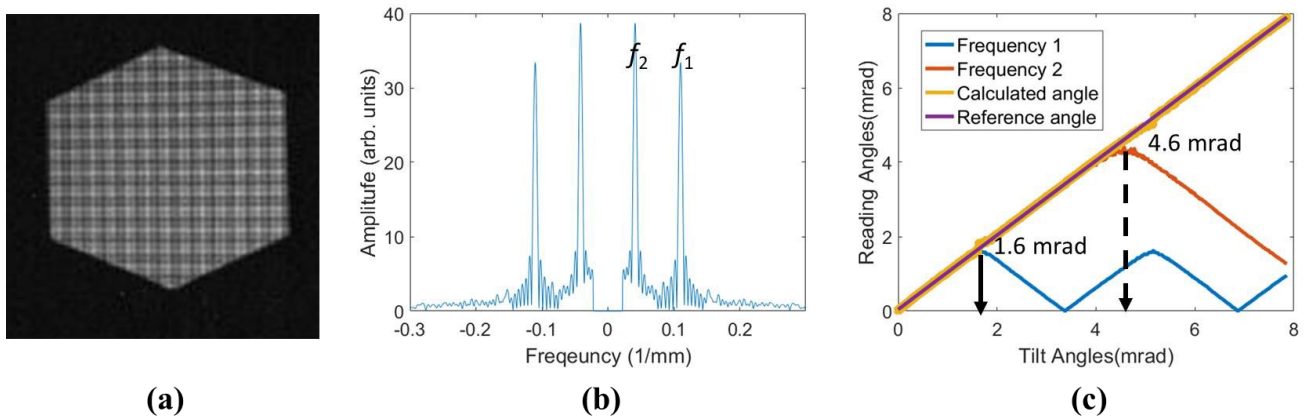

Fig. 5 (a) The snapshot of multiplexed fringe pattern that reflects in M4. (b) Two frequency component in the frequency domain. The unnecessary frequency bin near '0' was removed to simplify the data process. (c) The measurement results show the 2π ambiguity for Frequency 1 (Blue) and Frequency 2 (Red). The thick yellow line represents recovered calculation result using both frequency results and purple line represents the reference tilt angle based on motor's step number.

4. CONCLUSION

We developed the Simultaneous Multi-segmented mirror Orientation Test System (SMOTS) with an off-the-shelf camera and display. SMOTS measures multiple segmented mirrors simultaneously as long as the field of view of the camera can cover all the segments and each digital aperture has a sufficient sampling of the sinusoidal pattern. SMOTS can measure angular changes of a flat mirror with an RMS error of 0.8 µrad. Due to the simple and robust sheared sinusoidal pattern

approach, high-speed implementation (e.g., 15 Hz for seven hexagonal segments) is available for real-time monitoring or compensation. Finally, the multiplexing approach enables us to overcome the 2π ambiguity limit of SMOTS.

REFERENCES

[1] J. M. Oschmann, M. Clampin, H. MacEwen, "Special Section Guest Editorial: Space Telescopes," Opt. Eng. **52**(9), 0918019 (2013).
[2] J. S. Fender, "Future trends in large space optics," Proc. SPIE **4013**, 682–686 (2000).
[3] M. Johns, P. McCarthy, K. Raybould, A. Bouchez, A. Farahani, J. Filgueira, G. Jacoby, S. Shectman, and M. Sheehan, "Giant Magellan Telescope: overview," Proc. SPIE **8444**, 84441H (2012).
[4] R. Gilmozzi and J. Spyromilio, "The 42m European ELT: status," Proc. SPIE **7012**, 701219 (2008).
[5] N. Yaitskova and K. Dohlen, "Tip-tilt error for extremely large segmented telescopes: detailed theoretical pointspread-function analysis and numerical simulation results," J. Opt. Soc. Am. A **19**(7), 1274–1285 (2002).
[6] G. Chanan, M. Troy, F. Dekens, S. Michaels, J. Nelson, T. Mast, and D. Kirkman, ''Phasing the mirror segments of the Keck telescope: the broadband phasing algorithm,'' Appl. Opt. **37**, 140–155 (1998).
[7] J. M. Rodriguez-Ramos and J. J. Fuensalida, "Local Piston Detection of a Segmented Mirror Telescope with Curvature Sensing of Wavefronts Affected by Atmospheric Turbulence. Numerical Simulations," NATO ASI Ser., Ser. C **501**, 355–358 (1997).
[8] J. M. Rodriguez-Ramos, and J. J. Fuensalida, "Piston detection of a segmented mirror telescope using a curvature sensor: preliminary results with numerical simulations," Proc. SPIE **2871**, 613 (1997).
[9] N. Yaitskova, K. Dohlen, P. Dierickx, and L. Montoya, "Mach–Zehnder interferometer for piston and tip–tilt sensing in segmented telescopes: theory and analytical treatment," J. Opt. Soc. Am. A **22**, 1093–1105 (2005).
[10] X. Dai, O. Sasaki, J. E. Greivenkamp, and T. Suzuki, "High accuracy, wide range, rotation angle measurement by the use of two parallel interference patterns," Appl. Opt. **36**, 6190–6195 (1997)
[11] J. Yuan and X. Long, "CCD-area-based autocollimator for precision small-angle measurement," Rev. Sci. Instrum. **74**, 1362–1365 (2003).
[12] P. Su, R. E. Parks, L. Wang, R. P. Angel, and J. H. Burge, "Software configurable optical test system: a computerized reverse Hartmann test," Appl. Opt. **49**, 4404–4412 (2010).
[13] Y. Wu et. al., "Improved composite Fourier transform profilometry," Opt. and Laser Tech. **44**, 2037–2042 (2012).
[14] W. H. Southwell, "Wave-front estimation from wave-front slope measurements," J. Opt. Soc. Am. **70**(8), 998–1006 (1980).
[15] I. Trumper, H. Choi, and D. W. Kim, "Instantaneous phase shifting deflectometry," Opt. Express **24**, 27993–28007 (2016).
[16] L. Li, W. Zhao, F. Wu, and Y. Liu, "Flat mirror tilt and piston measurement based on structured light reflection," Opt. Express **22**, 27707–27716 (2014)
[17] H. Choi, I. Trumper, M. Dubin, W. Zhao, and D. W. Kim, "Simultaneous multi-segmented mirror orientation test system using a digital aperture based on sheared Fourier analysis," Opt. Express **25**, 18152-18164 (2017).

ACKNOWLEDGEMENT